Available online at www.sciencedirect.com
ScienceDirect
Trans. Nonferrous Met. Soc. China 25(2015) 2407−2414
Transactions of Nonferrous Metals Society of China
www.tnmsc.cn

Iron L-edge and sulfur K-edge XANES spectroscopy analysis of pyrite leached by *Acidianus manzaensis*

Hong-chang LIU[1, 2], Jin-lan XIA[1, 2], Zhen-yuan NIE[1, 2], Ya-long MA[1, 2], Chen-yan MA[3], Lei ZHENG[3], Cai-hao HONG[3], Yi-dong ZHAO[3]

1. School of Minerals Processing and Bioengineering, Central South University, Changsha 410083, China;
2. Key Laboratory of Biometallurgy of Ministry of Education of China, Central South University, Changsha 410083, China;
3. Institute of High Energy Physics, Chinese Academy of Sciences, Beijing 100049, China

Received 11 September 2014; accepted 17 November 2014

Abstract: Iron L-edge and sulfur K-edge X-ray absorption near edge structure (XANES) spectroscopy analysis of pyrite leached by extreme thermophilic Archaea strain *Acidianus manzaensis* (*A. manzaensis*) was carried out. Leaching experiments show that the oxidation of pyrite can be accelerated by *A. manzaensis*. Leaching results show that with the increase of leaching time, pH value in the leaching solution gradually decreases, redox potential increases rapidly from day 0 to day 3, and then increases slowly. The SEM results show that the pyrite surfaces are corroded gradually by *A. manzaensis*, and the XRD results show that the leaching residues contain new compositions of jarosite and elemental sulfur (S^0). The iron L-edge XANES spectroscopy analysis of pyrite during biooxidation indicates that pyrite is gradually converted to Fe(III)-containing species. The sulfur K-edge XANES spectroscopy analysis indicates that elemental sulfur is produced during bioleaching and maintains mass fractions of 3.2%−5.9%. Sodium thiosulfate was also detected from day 2 to day 4, indicating the existence of thiosulfate during biooxidation of pyrite.
Key words: pyrite; bioleaching; chemical speciation; XANES; *Acidianus manzaensis*

1 Introduction

Biohydrometallurgy takes important role in precious metal recovery from low grade mineral sulfide ores with attractive economical, environmental and social benefits [1]. Within these ores, pyrite is the most widely distributed and commonly coexists in coals, hydrothermal veins, contact metamorphic deposits and sedimentary rocks [2,3]. It has been widely studied that the biooxidation of pyrite can promote the extraction of inclusive gold and copper [4,5].

The dissolution kinetics and biooxidation mechanism of pyrite have been widely studied in recent years. According to VERA et al [6], pyrite can be initially attacked by Fe(III) and the sulfur moiety of pyrite is oxidized to sulfur intermediates, and then these sulfur intermediates can be finally oxidized to sulfate, which is well known as thiosulfate pathway, as presented in the following equations (Eqs. (1) and (2)). According to the mechanism, thiosulfate and other sulfur intermediates can be produced. Recently, there have been some publications focusing on the intermediate produced during bioleaching [7,8] and the intermediate sulfur has been confirmed [7,9]. However, these studies mostly concentrate on mesophiles (such as *Acidithiobacillus ferrooxidans*) and moderate thermophiles (such as *Sulfobacillus thermosulfidooxidans*) [3,10]. Up to now, only few publications concern on the dissolution of pyrite by extreme thermophilic Archaea strain, which shows high extraction rate of metal ions from metal sulfides [11]. In addition, it has been confirmed that the dissolution of surface sulfur-containing compounds may occur in different ways under different conditions during biooxidation of pyrite [12,13]. Therefore, it could be interesting to investigate the dissolution of pyrite by

Foundation item: Project (51274257) supported by the National Natural Science Foundation of China; Project (U1232103) supported by the Joint Funds of National Natural Science Foundation of China and Large Scientific Facility Foundation of Chinese Academy of Sciences; Project (CX2014B092) supported by the Hunan Provincial Innovation Foundation For Postgraduate, China; Project (VR-12419) supported by Beijing Synchrotron Radiation Facility Public User Program, China
Corresponding author: Jin-lan XIA; Tel: +86-731-8836944; E-mail: jlxia@csu.edu.cn
DOI: 10.1016/S1003-6326(15)63856-0

extreme thermophiles (such as *Acidianus manzaensis*).

$$FeS_2+6Fe^{3+}+3H_2O \longrightarrow S_2O_3^{2-}+7Fe^{2+}+6H^+ \quad (1)$$

$$S_2O_3^{2-}+8Fe^{3+}+5H_2O \longrightarrow 8Fe^{2+}+10H^++2SO_4^{2-} \quad (2)$$

On the other hand, the surface chemicals of sulfide minerals during bioleaching are so less abundant and/or unstable that they could be hardly detected [14]. This problem can be resolved by synchrotron radiation based X-ray absorption near edge structure (XANES) spectroscopy, which is efficient for analyzing composition and speciation transformation on surface of minerals [15,16]. In our previous study, sulfur K-edge XANES spectroscopy was used to study the surface sulfur speciation analysis during bioleaching of pyrite [17]. However, some important information in the dissolution process could be missed merely based on sulfur speciation. In order to learn the details of the dissolution, other chemical species transformation (i.e., Fe) during bioleaching should be also included.

In the present study, the Fe L-edge and S K-edge XANES spectroscopy patterns of pyrite leached by the typical extreme thermophilic Archaea strain *A. manzaensis* were analyzed. It could be useful for better understanding the dissolution mechanism of pyrite during bioleaching by thermophiles.

2 Experimental

2.1 Strain and culture medium

The strain *A. manzaensis* YN-25 (accession number of 16S rDNA in GeneBank: EF522787) was provided by the Key Laboratory of Biometallurgy of Ministry of Education of China, Changsha, China. The basal medium for cells' cultivation contained 3.0 g/L $(NH_4)_2SO_4$, 0.5 g/L $MgSO_4·7H_2O$, 0.5 g/L K_2HPO_4, 0.1 g/L KCl, 0.01 g/L $Ca(NO_3)_2$, and 0.2 g/L yeast extracts. The initial pH of the basal medium was adjusted to 1.7 with dilute sulfuric acid.

2.2 Mineral samples

The standard samples used in this research were provided by School of Minerals Processing and Bioengineering, Central South University, Changsha, China. X-ray fluorescence spectroscopy showed that the content of the original pyrite contained 45.68% S, 51.61% Fe, 1.74% Cu, 1.40% Si, 0.13% Mn, 0.11% Ca, 0.10% Al, 0.10% Mg, 0.05% As, 0.04% Pb and 0.03% K (mass fraction). Before the experiment, the original samples were ground to powder and passed through a sieve with hole diameter of 200−400 mesh and pretreated to remove the inorganic and organic matters from the mineral surface with water/ethanol solution (25% AR anhydrous ethanol and 75% sterilized ultrapure water) and acetone at room temperature.

2.3 Bioleaching experiment

The leaching experiment was carried out in the 500 mL flask containing 200 mL sterilized basal medium and 2 g pyrite in a high-temperature bath rotary shaker at 65 °C and 170 r/min. For bioleaching experiment by *A. manzaensis*, the initial inoculated cell density was 2×10^7 cell/mL. The abiotic control groups were performed without *A. manzaensis*. All above experiments were triplicate under the same conditions. During the experiment, the leaching parameters of total [Fe], $[Fe^{3+}]$, $[Fe^{2+}]$, pH, redox potential (Pt, vs SCE) and cell density were monitored at 24 h intervals. The total [Fe], $[Fe^{3+}]$ and $[Fe^{2+}]$ were determined by 5-sulfosalicylic acid spectrophotometry [18]; pH value was measured with a pH meter (PHS−3C); redox potential value was measured with a platinum (Pt) electrode, using a calomel electrode (Hg/Hg_2Cl_2) as reference; and the cell density was monitored by direct counting with a corpuscle counter.

2.4 Analysis methods

The surface morphology of pyrite residues was observed by the scanning electron microscopy (SEM) (Nova^{TM} NanoSEM 230, FEI, USA) according to the previous descriptions [15,16]. Leaching residues were characterized by XRD analysis using an X-ray diffractometer (DX 2000, Dandong Fangyuan Instrument Co., Ltd., China) with Cu K_α radiation (λ= 0.154 nm).

S K-edge and Fe L-edge XANES spectroscopy analyses were carried out at 4B7A beam-line and 4B7B beam-line, respectively, at Beijing Synchrotron Radiation Facility, Beijing, China, which were performed according to previous description [6,19]. Briefly, S K-edge XANES spectra data were recorded in the fluorescence mode at ambient temperature and scanned at step width of 0.2 eV between 2460 and 2490 eV. Fe L_3-edge XANES spectra data were recorded in the total electron yield (TEY) mode at the step widths of 0.5 eV from 690 to 703 eV and 0.1 eV from 705 to 928 eV. Then, these spectra were normalized to the maximum of the absorption spectrum and fitted for their linear combinations using known spectra from standard samples with IFEFFIT program [20].

3 Results and discussion

3.1 Leaching experiments

The leaching experiments of pyrite by *A. manzaensis* in sterile control groups were performed in terms of the cell density, pH and redox potential value, total [Fe], $[Fe^{2+}]$ and $[Fe^{3+}]$ (Figs. 1(a)−(d)). The results in Fig. 1(a) show that, during bioleaching of pyrite by *A.*

manzaensis, the cell density increases from day 0 to day 2 reaching the stationary phase with cell density of 2.5×10^8 cell/mL, and then decreases from day 3.5. The pH value of the culture solution decreases continuously, and reaches 1.14 after 5 days' bioleaching. The redox potential value increases rapidly from day 0 to day 3 and then increases slowly. Results in Fig. 1(b) show that both total [Fe] and [Fe^{3+}] increased with prolonging time, while total [Fe] was slightly higher than [Fe^{3+}] from day 0 to day 2.5 and then was basically the same. [Fe^{2+}] slightly increases from day 0 to day 0.5, reaching the maximum value of 0.12 g/L, and then decreases to approach zero. By contrast, results in Fig. 1(c) show that, in the sterile control groups, the pH value decreases rapidly from 1.70 to 1.64 at day 0−0.5 and then slowly decreases to reach 1.60. The redox potential value gradually increases from 348 to 355 mV. Results in Fig. 1(d) show that total [Fe] and [Fe^{2+}] increase fast initially and then increase slowly. Meanwhile, [Fe^{3+}] is basically zero.

According to previous descriptions [3,6], proton and ferrous ion can be formed during the oxidation of pyrite, as shown in Eqs. (3) and (4), which probably lead to the decrease of pH value in Figs. 1(a) and (c), and the increase of [Fe^{2+}] in the initial stage (Figs. 1(b) and (d)) during leaching of pyrite. However, ferrous ions can be rapidly oxidized to ferric ions with the growth of *A. manzaensis* cells (Eq. (5)), which can accelerate the dissolution of pyrite (Eq. (2)). It should be noted that with the increase of ferric ions, the formation of jarosite could be also accelerated (Eq. (6)). Previous study indicated that the accumulation of jarosite on the surface of minerals could hinder the dissolution [21], which could be one of the reasons for the slowing down of the redox potential value and cell growth.

$$2FeS_2+2H_2O+7O_2\longrightarrow 2Fe^{2+}+4SO_4^{2-}+4H^+ \quad (3)$$

$$FeS_2+8H_2O+14Fe^{3+}\longrightarrow 15Fe^{2+}+2SO_4^{2-}+16H^+ \quad (4)$$

$$4Fe^{2+}+4H^++O_2\longrightarrow 4Fe^{3+}+2H_2O \quad (5)$$

$$M^++3Fe^{3+}+2SO_4^{2-}+6H_2O\longrightarrow MFe_3(SO_4)_2(OH)_6+6H^+ \quad (6)$$

where M is a monovalent cation, such as H_3O^+, K^+, Na^+ and NH_4^+.

3.2 Surface morphology and composition analysis

The surface morphologies of the pyrite residues bioleached by *A. manzaensis* and in the sterile control experiment are observed by SEM (Fig. 2). Results in

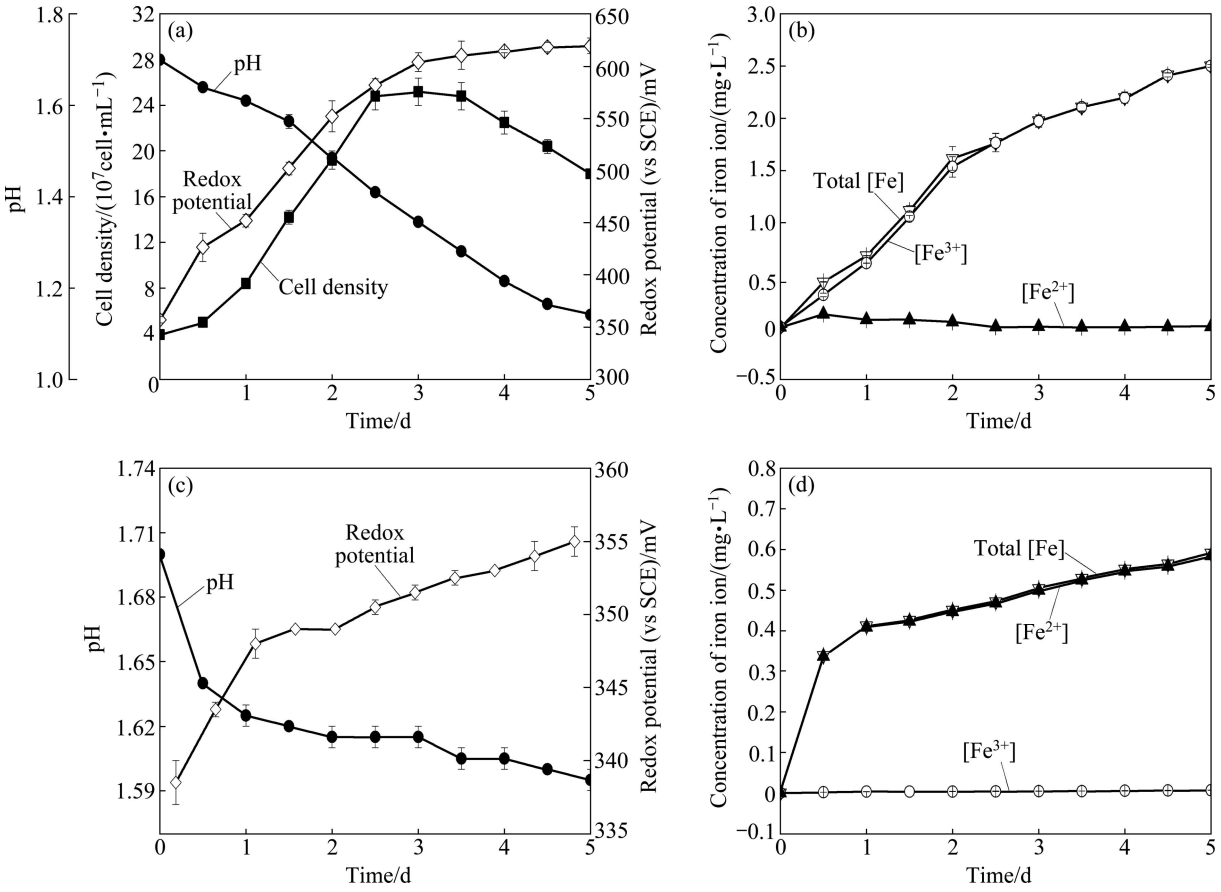

Fig. 1 Leaching behavior of pyrite with *A. manzaensis* (a,b) and in sterile control experiment (c,d) (■ Cell density; ● pH; ◇ Redox potential; ▽ Total [Fe]; ○ [Fe^{3+}]; ▲ [Fe^{2+}])

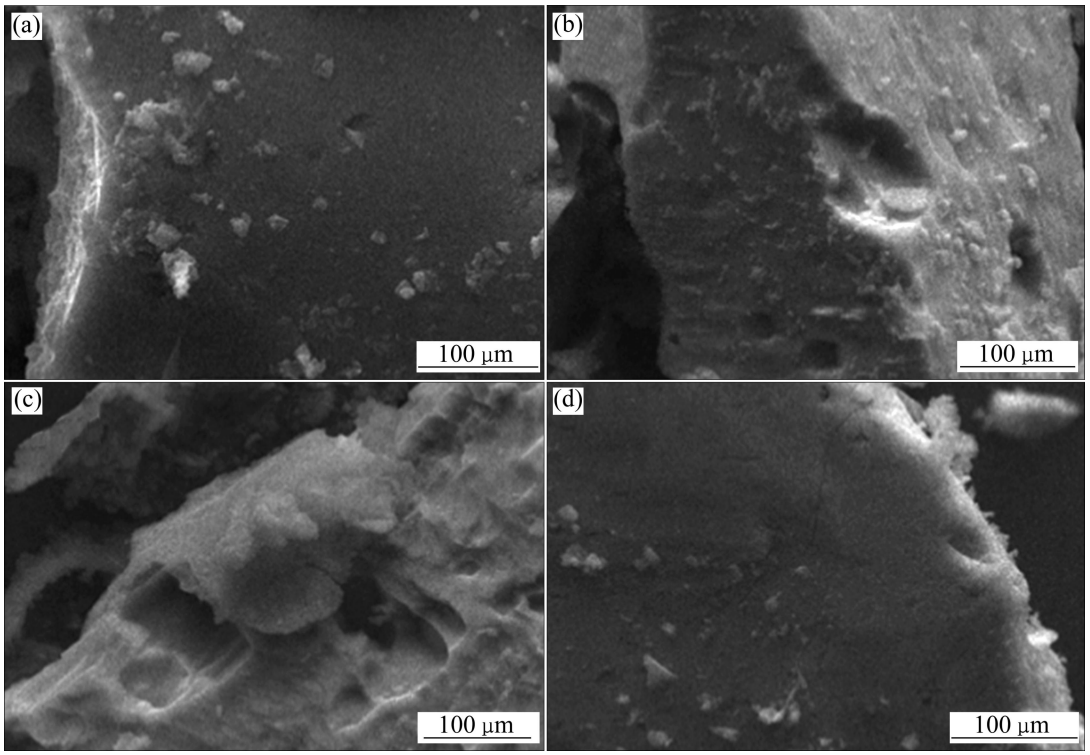

Fig. 2 SEM micrographs of pyrite particles leached by *A. manzaensis* cells after 0 d (a), 2 d (b) and 5 d (c), and in sterile control experiment (d)

Figs. 2(b) and (c) show that the surfaces of pyrite are corroded gradually by *A. manzaensis*, and the surface of the leaching residue at day 5 (Fig. 2(c)) becomes rough compared with the original pyrite (Fig. 2(a)). By contrast, results in Fig. 2(d) show that few products form in sterile control experiment and the surface morphologies are basically unchanged compared with the original pyrite.

The XRD patterns of original pyrite and pyrite residue leached by *A. manzaensis* and chemically leached in the sterile controls are shown in Figs. 3(a)−(c), respectively. Compared with the XRD pattern of original pyrite (Fig. 3(a)), the XRD pattern of bioleaching residues (Fig. 3(b)) shows new peaks corresponding to jarosite and elemental sulfur (S^0) appears. While no obvious change occurs in the sterile control experiment (Fig. 3(c)).

3.3 Iron L-edge and sulfur K-edge XANES spectroscopy analysis of pyrite leached by *A. manzaensis*

In order to study the iron and sulfur speciation during bioleaching, Fe L-edge XANES spectroscopy and S K-edge XANES spectroscopy are used, respectively. The Fe L-edge XANES spectra of the standard samples (pyrite (FeS_2); ferrous sulfate ($FeSO_4$); ferroferric oxide (Fe_3O_4); ferric sulfate ($Fe_2(SO_4)_3$), jarosite ($KFe_3(SO_4)_2(OH)_6$) and pyrite leached by *A. manzaensis* and in the sterile control experiment are shown in Figs. 4(a) and (b), respectively. It can be seen from Fig. 4(a) that there is a significant difference in the shape of the L_3-edge and the L_2-edge. For iron L_3-edge, the intensity of peak *a* for ferrous sulfate (Fe(II)) is significantly higher than that of peak *b*. Instead, the intensity of peak *b* for ferric sulfate (Fe(III)) is significantly higher than that of peak *a*. It can also be seen from Fig. 4(a) that the L_2-edge for Fe(II) is higher than that for Fe(III). In the case of ferroferric oxide, the situation is between ferrous sulfate and ferric sulfate. The Fe L-edge XANES spectra of the original pyrite and the produced jarosite during bioleaching of pyrite show the similar features of the L_3-edge and L_2-edge for Fe(II) and Fe(III), respectively, which are also consistent with previous description [22]. Previous study indicated that the formation of Fe(III) on the mineral surface should result in an increase in the branching ratio, $I(L_{III})/[I(L_{II})/I(L_{III})]$, as iron changes from low-spin Fe(II) to high-spin Fe(III) [23]. This indicates that the increase of the intensity of peak *b* accompanied with the decrease of the intensity peaks *a* and *c* can reflect the conversion of Fe(II) speciation to Fe(III) speciation.

Results in Fig. 4(b) show that the intensity of peak *a* is gradually decreased with prolonging time during bioleaching, while the intensity of peak *b* is gradually

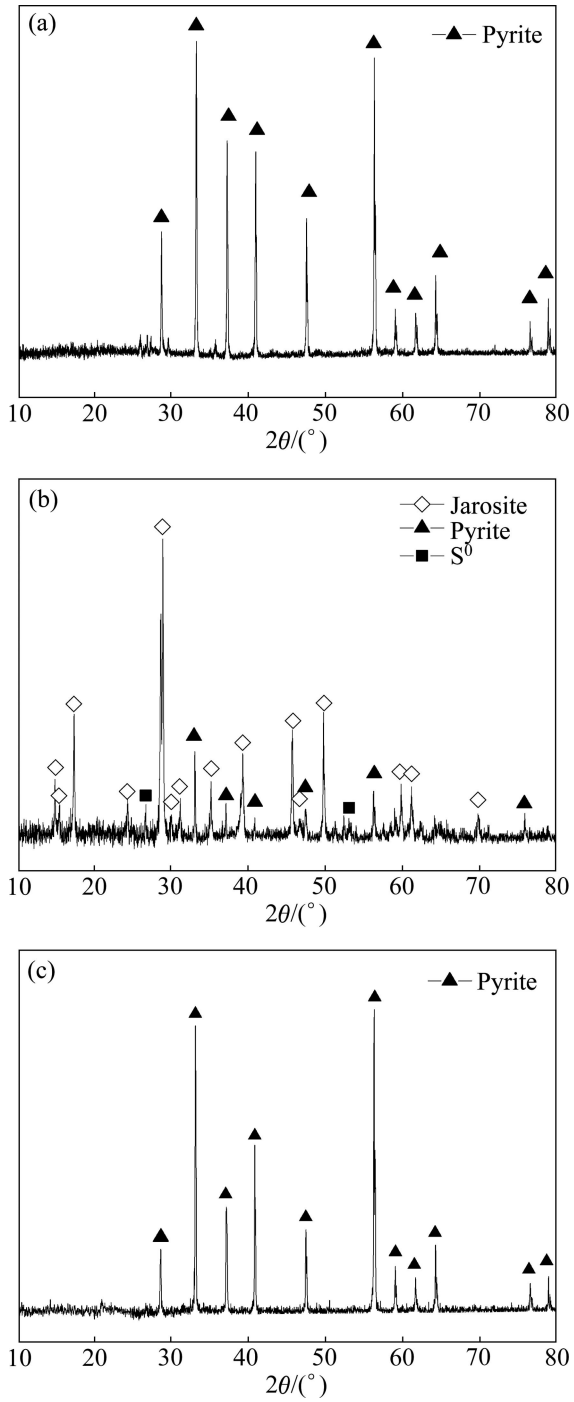

Fig. 3 XRD patterns of original pyrite (a) and pyrite residue leached by *A. manzaensis* (b) and chemically leached in sterile controls (c)

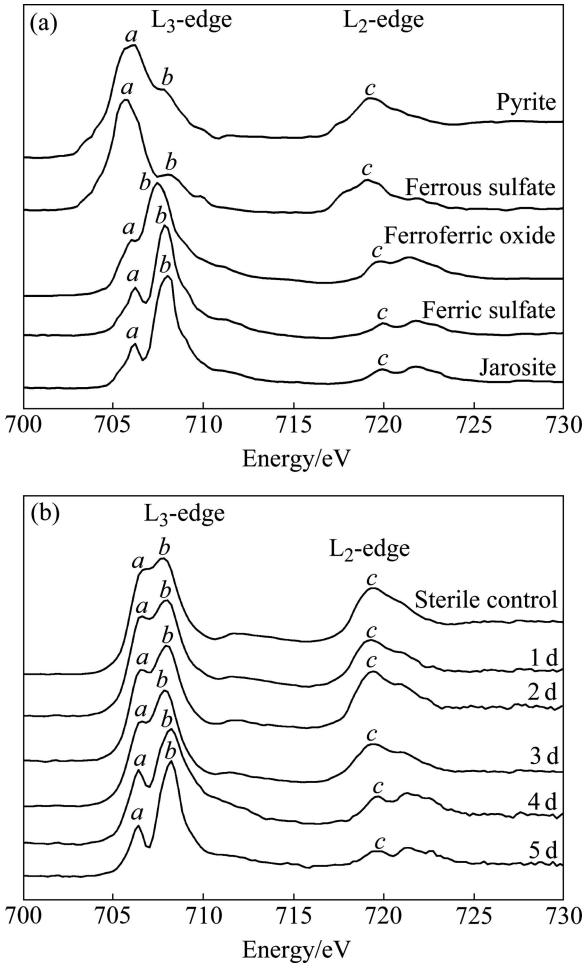

Fig. 4 Iron L-edge XANES spectra of standard samples (a) and pyrite residues leached by *A. manzaensis* for 1, 2, 3, 4 and 5 d, and leached chemically for 5 d (b) (*a* and *b* represents low energy shoulder and high energy shoulder of L_3-edge, respectively; *c* represents L_2-edge)

increased, meanwhile the intensity of peak *c* is also gradually increased. This indicated the increase of Fe(III) speciation and the decrease of Fe(II) speciation on the surface of pyrite during bioleaching. It should be noted that the spectra of pyrite bioleached at day 5 are similar to those of original pyrite, indicating that pyrite is mostly converted to Fe(III)-containing species. In addition, compared with the spectra of original pyrite (Fig. 4(a)), the spectra of pyrite after chemically leaching for 5 d in the sterile control experiment show the existence of Fe(III) on the mineral surface, which may result from the oxidation of pyrite by Eq. (5).

The sulfur K-edge XANES spectra of the standard samples and pyrite leached by *A. manzaensis* and in the sterile control experiment are shown in Figs. 5(a) and (b), respectively. It can be seen from Fig. 5(a) that the XANES spectra of standard samples (pyrite FeS_2, elemental sulfur S^0, oxidized glutathione GSSG, reduced glutathione GSH, sodium tetrathionate $Na_2S_4O_6$, sodium thiosulfate $Na_2S_2O_3$, sodium sulfite, Na_2SO_3, jarosite $KFe_3(SO_4)_2(OH)_6$)) show significant difference in the position intensity and width of the absorption peaks, which are in accordance with previous descriptions [17]. Results in Fig. 5(b) show that, compared with the spectra of original pyrite, the XANES spectra of pyrite leached

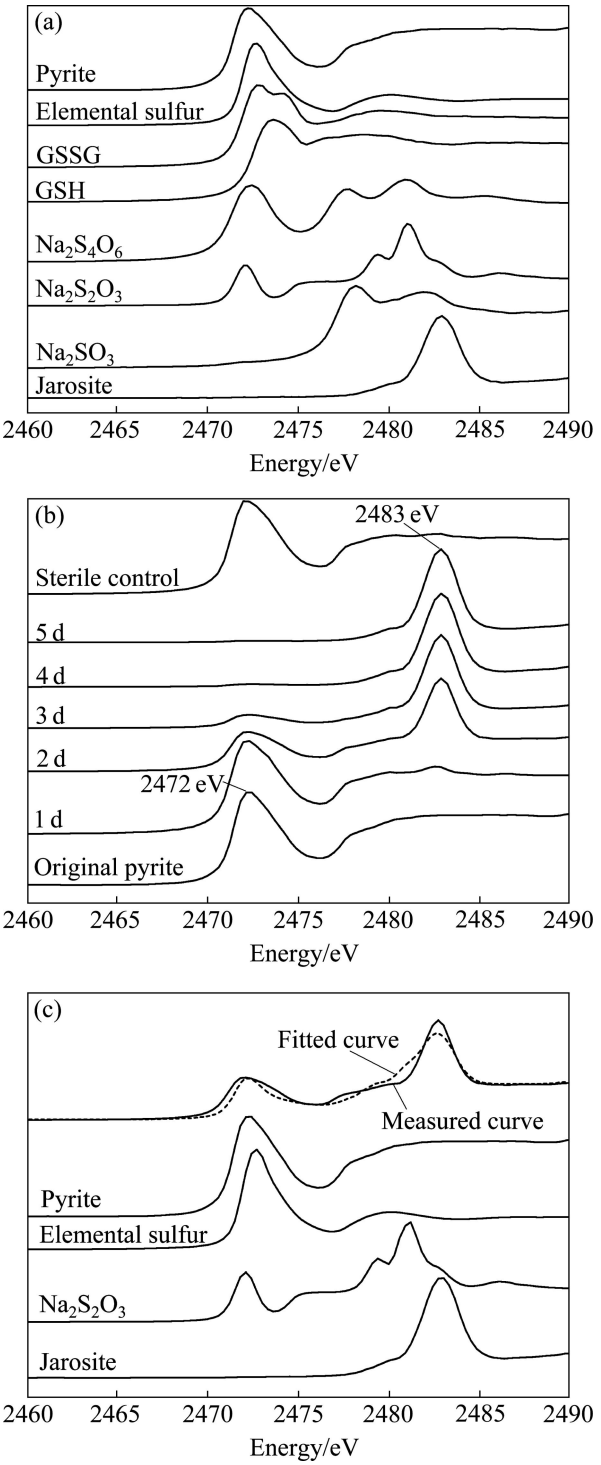

Fig. 5 Normalized sulfur K-edge XANES spectra of standard samples (a), spectra of original pyrite and pyrite leached by *A. manzaensis* and in sterile control experiment (b), and fitted spectra of pyrite leached for 2 d by *A. manzaensis* (c) (Abbreviations of GSSG and GSH in (a) represent oxidized glutathione and reduced glutathione, respectively)

by *A. manzaensis* change overtime, in which the peak at 2472 eV becomes weaker overtime and finally basically disappears, and the peak at 2483 eV gradually appears and finally becomes the main peak. By contrast, little change is found from the spectra of pyrite residues in the sterile control experiment.

In order to quantify sulfur speciation composition, the S K-edge XANES spectra of these unknown samples (Fig. 5(b) are fitted for their linear composition using the standard spectra of sulfur-compounds (Fig. 5(a)), respectively. The fitted spectra of pyrite leached for 2 d and the fitted results of pyrite leached at different time by *A. manzaensis* are shown in Fig. 5(c) and Table 1, respectively. Results in Table 1 show that during bioleaching, the amount of pyrite gradually decreases, and after bioleaching for 5 d the residue contains only 4.2% pyrite. Elemental sulfur is produced during bioleaching and maintains mass fractions at 3.2%−5.9%. Jarosite gradually increases and finally reaches mass fraction of 89%. The decrease of pyrite and the increase of jarosite probably are caused by the rapid increase of ferric ion during bioleaching (Fig. 1(b)), which should be contributed to the increase of Fe(III) speciation and the decrease of Fe(II) speciation in Fig. 4(b), which is also consistent with XRD results (Fig. 3(c)).

Table 1 Fitted results of S K-edge XANES spectra of pyrite treated by *A. manzaensis* with different reference standard spectra

Sample	Contribution of standard spectra/%			
	Pyrite	S^0	Jarosite	$Na_2S_2O_3$
In sterile control	96.8	1.7	1.5	−
Bioleaching for 1 d	89.3	3.2	7.5	−
Bioleaching for 2 d	52.8	5.1	38.8	3.3
Bioleaching for 3 d	18.7	5.7	71.1	4.5
Bioleaching for 4 d	8.0	5.5	83.3	3.2
Bioleaching for 5 d	4.2	5.9	89.9	−

It should be noted that sodium thiosulfate is also detected at day 2 to day 4, which is in agreement with XIA et al [17], indicating that sodium thiosulfate is formed as an important intermediate compound during bioleaching of pyrite (Eq. (1)). According to previous descriptions [6,24], the thiosulfate specie, which might bind to the pyrite surface as Py—S—SO_3 (Py represents pyrite), can be formed with the oxidation of the sulfur moiety of pyrite, and has been proposed by BORDA et al [25,26]. The decomposition of Py—S—SO_3 may occur as Eq. (7) [17]. In addition, with the formation of thiosulfate, elemental sulfur can be formed (Eq. (8)), indicating the existence of elemental sulfur and thiosulfate during biooxidation of pyrite.

$$Py—S—SO_3 \longrightarrow Py+MS_2O_3 \quad (7)$$

$$S_2O_3^{2-}+2H^+ \longrightarrow S^0+H_2SO_3 \quad (8)$$

4 Conclusions

1) Bioleaching experiment shows that the oxidation of pyrite can be accelerated by *A. manzaensis*.

2) Compared with the original pyrite, the surfaces of pyrite are corroded gradually by *A. manzaensis*. The XRD patterns of bioleaching residues show the leaching residues contain new compositions of jarosite and elemental sulfur (S^0).

3) The iron L-edge XANES spectroscopy analysis of pyrite during biooxidation indicates that pyrite is gradually converted to Fe(III)-containing species.

4) The sulfur K-edge XANES spectroscopy analysis indicates that during bioleaching, pyrite gradually decreases and jarosite gradually increases. Elemental sulfur is produced during bioleaching and maintains mass fractions of 3.2%−5.9%. Interestingly, sodium thiosulfate is also detected, indicating the existence of thiosulfate during biooxidation of pyrite.

References

[1] BRIERLEY C L. Biohydrometallurgical prospects [J]. Hydrometallurgy, 2010, 104(3−4): 324−328.

[2] CHANDRAPRABHA M, NATARAJAN K. Surface chemical and flotation behaviour of chalcopyrite and pyrite in the presence of *Acidithiobacillus thiooxidans* [J]. Hydrometallurgy, 2006, 83(1): 146−152.

[3] ZHANG X, GU G H, HU K T, WANG C Q. Bioleaching behavior and surface property of pyrites in different metallogenic conditions [J]. Chinese Journal of Geochemistry, 2014, 33(3): 256−261.

[4] GROUDEV S, SPASOVA I, IVANOV I. Two-stage microbial leaching of a refractory gold-bearing pyrite ore [J]. Minerals Engineering, 1996, 9(7): 707−713.

[5] ZHANG Jie, WU Ai-xiang. Research on enhancing dump leaching of chalcopyrite by pyrite [J]. Metal Mine, 2008, 3: 38−41. (in Chinese)

[6] VERA M, SCHIPPERS A, SAND W. Progress in bioleaching: Fundamentals and mechanisms of bacterial metal sulfide oxidation—part A [J]. Applied Microbiology and Biotechnology, 2013, 97(17): 7529−7541.

[7] BALCI N, MAYER B, SHANKS III W C, MANDERNACK K W. Oxygen and sulfur isotope systematics of sulfate produced during abiotic and bacterial oxidation of sphalerite and elemental sulfur [J]. Geochimica et Cosmochimica Acta, 2012, 77: 335−351.

[8] DEMOISSON F, MULLET M, HUMBERT B. Pyrite oxidation in acidic medium: Overall reaction pathway [J]. Surface and Interface Analysis, 2008, 40(3−4): 343−348.

[9] HANSFORD G, VARGAS T. Chemical and electrochemical basis of bioleaching processes [J]. Hydrometallurgy, 2001, 59(2−3): 13−26.

[10] LIU H, GU G H, XU Y B. Surface properties of pyrite in the course of bioleaching by pure culture of *Acidithiobacillus ferrooxidans* and a mixed culture of *Acidithiobacillus ferrooxidans* and *Acidithiobacillus thiooxidans* [J]. Hydrometallurgy, 2011, 108(1−2): 143−148.

[11] HE Huan, YANG Yi, XIA Jin-lan, DING Jian-nan, ZHAO Xiao-juan, NIE Zhen-yuan. Growth and surface properties of new thermoacidophilic Archaea strain *Acidianus manzaensis* YN-25 grown on different substrates [J]. Transactions of Nonferrous Metals Society of China, 2008, 18(6): 1374−1378.

[12] NEMATI M, LOWENADLER J, HARRISON S. Particle size effects in bioleaching of pyrite by acidophilic thermophile *Sulfolobus metallicus* (BC) [J]. Applied Microbiology and Biotechnology, 2000, 53(2): 173−179.

[13] YAHYA A, JOHNSON D B. Bioleaching of pyrite at low pH and low redox potentials by novel mesophilic Gram-positive bacteria [J]. Hydrometallurgy, 2002, 63(2): 181−188.

[14] FERRER S, PETROFF Y. Surface science done at third generation synchrotron radiation facilities [J]. Surface Science, 2002, 500(1−3): 605−627.

[15] XIA J L, YANG Y, HE H, LIANG C L, ZHAO X J, ZHENG L, MA C Y, ZHAO Y D, NIE Z Y, QIU G Z. Investigation of the sulfur speciation during chalcopyrite leaching by moderate thermophile *Sulfobacillus thermosulfidooxidans* [J]. International Journal of Mineral Processing, 2010, 94(1−2): 52−57.

[16] LIU H C, XIA J L, NIE Z Y, PENG A A, MA C Y, ZHENG L, ZHAO Y D. Comparative study of sulfur utilization and speciation transformation of two elemental sulfur species by thermoacidophilic Archaea *Acidianus manzaensis* YN-25 [J]. Process Biochemistry, 2013, 48(12): 1855−1860.

[17] XIA J L, YANG Y, HE H, ZHAO X J, LIANG C L, ZHENG L, MA C Y, ZHAO Y D, NIE Z Y, QIU G Z. Surface analysis of sulfur speciation on pyrite bioleached by extreme thermophile *Acidianus manzaensis* using Raman and XANES spectroscopy [J]. Hydrometallurgy, 2010, 100(3−4): 129−135.

[18] KARAMANEV D G, NIKOLOV L N, MAMATARKOVA V. Rapid simultaneous quantitative determination of ferric and ferrous ions in drainage waters and similar solutions [J]. Minerals Engineering, 2002, 15(5): 341−346.

[19] HE H, XIA J L, YANG Y, JIANG H C, XIAO C Q, ZHENG L, MA C Y, ZHAO Y D, QIU G Z. Sulfur speciation on the surface of chalcopyrite leached by *Acidianus manzaensis* [J]. Hydrometallurgy, 2009, 99(1−2): 45−50.

[20] RAVEL B, NEWVILLE M. ATHENA, ARTEMIS, HEPHAESTUS: Data analysis for X-ray absorption spectroscopy using IFEFFIT [J]. Journal of Synchrotron Radiation, 2005, 12(4): 537−541.

[21] KLAUBER C. A critical review of the surface chemistry of acidic ferric sulphate dissolution of chalcopyrite with regards to hindered dissolution [J]. International Journal of Mineral Processing, 2008, 86(1−4): 1−17.

[22] MOSSELMANS J, PATTRICK R, van der LAAN G, CHARNOCK J, VAUGHAN D, HENDERSON C, GARNER C. X-ray absorption near-edge spectra of transition metal disulfides FeS_2 (pyrite and marcasite), CoS_2, NiS_2 and CuS_2, and their isomorphs FeAsS and CoAsS [J]. Physics and Chemistry of Minerals, 1995, 22(5): 311−317.

[23] THOLE B, van der LAAN G. Branching ratio in X-ray absorption spectroscopy [J]. Physical Review B, 1988, 38(5): 3158.

[24] RIMSTIDT J D, VAUGHAN D J. Pyrite oxidation: A state-of-the-art assessment of the reaction mechanism [J]. Geochimica et Cosmochimica Acta, 2003, 67(5): 873−880.

[25] BORDA M J, STRONGIN D R, SCHOONEN M A. A vibrational spectroscopic study of the oxidation of pyrite by molecular oxygen [J]. Geochimica et Cosmochimica Acta, 2004, 68(8): 1807−1813.

[26] BORDA M J, STRONGIN D R, SCHOONEN M A. A vibrational spectroscopic study of the oxidation of pyrite by ferric iron [J]. American Mineralogist, 2004, 88(8−9): 1318−1323.

Acidianus manzaensis 浸出黄铁矿过程中铁 L 边和硫 K 边 XANES 光谱学分析

刘红昌[1,2]，夏金兰[1,2]，聂珍媛[1,2]，马亚龙[1,2]，马陈燕[3]，郑　雷[3]，洪才浩[3]，赵屹东[3]

1. 中南大学 资源加工与生物工程学院，长沙 410083；
2. 中南大学 生物冶金教育部重点实验室，长沙 410083；
3. 中国科学院 高能物理研究所，北京 100049

摘　要：基于同步辐射技术对 *Acidianus manzaensis* (*A. manzaensis*)浸出黄铁矿过程中铁 L 边 XANES 和硫 K 边 XANES 进行光谱学分析。浸出实验表明，*A. manzaensis* 能加速黄铁矿的氧化。随着浸出时间的增加，浸出液的 pH 值逐渐降低；氧化还原电位值在第 0~3 天快速增加，然后缓慢增加。SEM 结果表明，黄铁矿表面被 *A. manzaensis* 逐渐腐蚀；XRD 结果表明，浸出残渣包含新组分黄钾铁矾和单质硫。铁 L 边 XANES 光谱学分析表明，黄铁矿生物氧化过程中铁形态逐渐转变为含 Fe(III)物质。硫 K 边 XANES 光谱学分析表明，在黄铁矿生物浸出过程中产生元素硫且其质量比维持在 3.2%~5.9%。硫代硫酸盐在第 2~4 天也被检测出来，这表明黄铁矿生物浸出过程中存在硫代硫酸盐。

关键词：黄铁矿；生物浸出；化学形态；XANES；*Acidianus manzaensis*

(Edited by Wei-ping CHEN)